Modelling of vacuum membrane distillation

Zhang, Jianhua, Li, Jun-de, Duke, Mikel, Hoang, Manh, Zongli, Xie, Groth, Andrew, Tun, Chan and Gray, Stephen (2013) Modelling of vacuum membrane distillation. Journal of Membrane Science, 434. pp. 1-9. ISSN 0376-7388

www.elsevier.com/locate/memsci

Modelling of vacuum membrane distillation

Jianhua Zhang, Jun-De Li, Mikel Duke, Manh Hoang, Zongli Xie, Andrew Groth, Chan Tun, Stephen Gray

PII: S0376-7388(13)00085-9
DOI: http://dx.doi.org/10.1016/j.memsci.2013.01.048
Reference: MEMSCI11912

To appear in: *Journal of Membrane Science*

Received date: 7 October 2012
Revised date: 11 January 2013
Accepted date: 14 January 2013

Cite this article as: Jianhua Zhang, Jun-De Li, Mikel Duke, Manh Hoang, Zongli Xie, Andrew Groth, Chan Tun and Stephen Gray, Modelling of vacuum membrane distillation, *Journal of Membrane Science,* http://dx.doi.org/10.1016/j.memsci.2013.01.048

Modelling of Vacuum Membrane Distillation

Jianhua Zhang[a]*, Jun-De Li[b], Mikel Duke[a], Manh Hoang[c], Zongli Xie[c], Andrew Groth[d], Chan Tun[d], Stephen Gray[a]

[a] Institute of Sustainability and Innovation, Victoria University, PO Box 14428, Melbourne, Victoria 8001, Australia
[b] School of Engineering and Science, Victoria University, P.O. Box 14428, Melbourne, Victoria 8001, Australia
[c] CSIRO Materials Science & Engineering, Private bag 33, Clayton South MDC, Victoria 3169, Australia
[d] R&D, Memcor, Siemens, 15 Blackman Crescent, South Windsor, New South Wales, 2756, Australia

* Corresponding author. Tel.: +61 3 9919 7617; fax: +61 3 9919 7696. E-mail address: jianhua.zhang@vu.edu.au

Abstract

A new method of measuring the properties of hollow fibre membranes for modelling purposes was developed. Measuring the gas permeability as a function of membrane length and extrapolating to zero length provided enough membrane material information for modelling the flux. These values resulted in the predicted Vacuum Membrane Distillation (VMD) flux within the experimental errors (±5%) for different velocities. The predicted results at different temperatures were mostly within the experimental variation range. However, the error (<10%) was greater at the highest temperature tested, perhaps due to water evaporation in the feed tank. Additionally both the modelling and experimental results show that the flux in VMD was independent of the module packing density under the presented conditions. The results also show that the mathematical model predictions agree well with the experimental results of short experimental duration (1 - 2 h).

Key words:

Membrane distillation, modelling, gas permeation, hollow fibre membrane

1. Introduction

Membrane distillation (MD) is a hybrid of thermal distillation and membrane separation [1]. The concept of MD was first described in technical literature in 1967 [2], and numerous researchers around the world have contributed to the understanding of the process [3, 4]. MD is a thermal, membrane-based separation process [3, 4]. Although a membrane is involved in MD, the driving force is quite different from other membrane processes, being the vapour pressure difference across the membrane which drives mass transfer through a membrane [3, 5], rather than an applied absolute pressure difference, a concentration gradient or an electrical potential gradient.

MD has 100% theoretical rejection of non-volatile components and can utilise low grade heat sources of 40 - 80 °C. It is a well known process for concentrate treatment at low temperature, because MD is not significantly affected by concentration polarization as are nanofiltration and Reverse Osmosis (RO) [3]. In MD, hydrophobic membranes (pore size approximately in the range of 0.1 - 1 μm) [6] are in direct contact with the aqueous feed solutions and are employed as a barrier between the feed and the product water. Furthermore, the membrane should not be wetted by the process liquids, no capillary condensation should take place inside the pores of the membrane, and only vapour should be transported through the membrane [3]. Although MD still suffers from fouling problems [7], it shows much better fouling resistance than RO. In addition, MD can be conveniently integrated with conventional RO processes to increase the recovery ratio of desalted water and/or improve the energy

efficiency of the system [8], to reduce the footprint of evaporation ponds or even substitute for the evaporation pond in processing the RO concentrate. The possibility of using plastic equipment also reduces or avoids corrosion problems.

In comparison with other thermal desalination technology (i.e. Multiple Stage Flash), the path length of the vapour phase in MD is approximately the membrane thickness (~100 μm), which is much shorter. It is potentially a commercial desalination technique if it can be combined with solar energy, geothermal energy or waste heat available in power stations or chemical plants. However, if low cost thermal energy is not available or in low supply, as a thermal distillation process, MD is also an energy intensive technique. Hence, a significant improvement of Gain Output Ratio (GOR) is required for effective production of fresh water. The economics of thermal processes with the trade off between thermal efficiency and plant capital cost is well described [9]. A high GOR is not always economically viable because of the added plant capital required to recycle heat. MD has similar economics and careful considerations should be put towards the cost and abundance of the thermal energy in deciding the best MD configuration and GOR.

The four major configurations of MD process are shown in Figure 1, including direct contact membrane distillation (DCMD), air gap membrane distillation (AGMD), VMD and sweep gas membrane distillation (SGMD). The difference among these four configurations is the status of the permeate side. In Figure 1, T_f and T_p are the feed and permeate bulk temperatures, T_1 and T_2 are the membrane interface temperatures on the feed and permeate sides, P_f and P_p are the hydraulic pressures on the feed permeate sides, P_{vacuum} is the pressure in the vacuum chamber, and P_{vapour} is the vapour pressure at the membrane interface on the feed side.

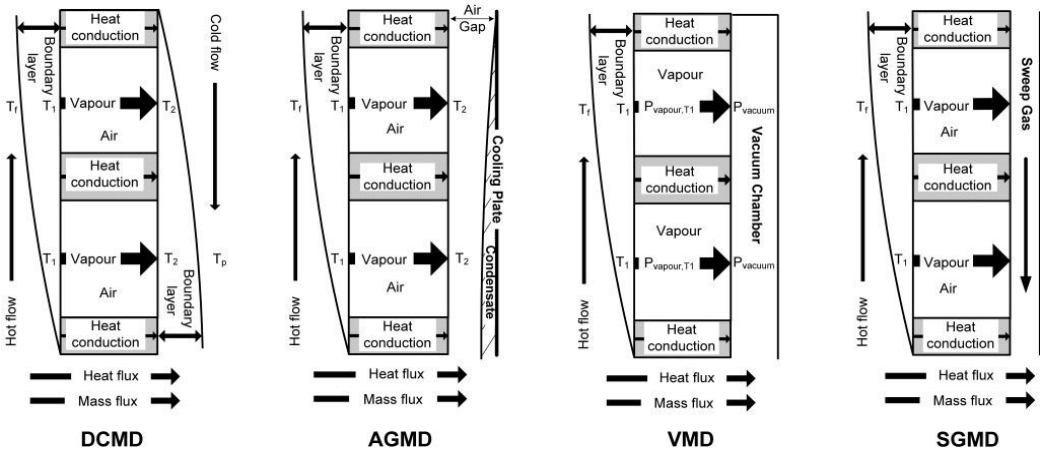

Figure 1 Configurations for membrane distillation

In VMD, the permeate side is under reduced pressure maintained below the equilibrium vapour pressure of the feed by a vacuum pump, and the vapour permeate is drawn out of the chamber and condenses in an external condenser. Furthermore, the difference between the hydrodynamic pressure of the feed stream and pressure in the pores should not be greater than the minimum Liquid Entry Pressure (*LEP*).

The mass transfer in VMD is characterised as occurring in via single-gas convective mass flow as non-condensable gases that maybe present are removed by absolute pressure drop across the membrane (i.e. the saturated vapour pressure at feed/membrane interface and the vacuum pressure at permeate/membrane interface). In contrast, mass transfer in DCMD and AGMD is characterised by mass diffusion in a gas mixture due to the presence of non-condensable gases within the pores, and the driving force is the vapour pressure difference across the pores. There is no convective mass flow in the pores (total pressure difference in the pores equals zero) for DCMD or AGMD. Therefore, the mass flux of VMD is generally larger than that of other MD configurations if the vapour pressure difference across the membrane is the same. Another advantage of the VMD comes from the negligible heat conduction through the membrane [4], due to the very low vapour pressure on the permeate side of the membrane. This advantage makes VMD highly thermal efficient and simplifies the mathematical models describing VMD. However, it is found that VMD is the least studied among the four available MD configurations, with only about 8% of the published MD references focused on VMD [4]. Also, membrane wetting potential in VMD is probably higher than that of other MD configurations due to the higher absolute pressure difference across the membrane, and vacuum pumps are generally energy inefficient compared to hydraulic pumps.

In this study, hollow fibre VMD was modelled and assessed experimentally. In conventional VMD modelling, membrane characteristics such as pore size, tortuosity, membrane thickness and porosity are the essential parameters [10]. Woods et al. [11] also showed that pore size distribution had greater influence on predicting results for VMD than that of the other MD configurations. However, these membrane characteristics are not always readily available for accurate modelling due to the limitations of characterisation techniques. For example, because the MD membrane is generally more porous than filtration membranes and can be compressed under normal operating pressure [12, 13], characterisation methods such as mercury porosimetry are not accurate. Gas permeability is useful for measuring flat sheet membranes, but will show large errors when used for hollow fibre membranes due to the length dependency of the gas flux. In this paper, the characteristics needed for modelling was analysed based on the mass transfer mechanism across the membrane in VMD, and it was found that it was not necessary to measure the traditional parameters used in conventional VMD modelling. Rather, a new and simple approach in VMD modelling is developed, which is validated experimentally.

2. Theoretical analysis of mass transfer mechanism in VMD

2.1 Mass transfer

The mass transfer through a porous MD membrane can be interpreted by three fundamental mechanisms: Knudsen diffusion, molecular diffusion and Poiseuille flow [14, 15]. The Knudsen number (Kn):

$$Kn = l / d \tag{1}$$

is used to judge the dominating mechanism of the mass transfer in the pores. Here, l is the mean free path of the transferred gas molecules and d is the mean pore diameter of the membrane.

For VMD, it can be assumed that a single gas (water vapour) is contained in the membrane pores (this may be affected by the total dissolved carbonate in the feed water), and the driving force is the pressure difference across the membrane between the saturated vapour pressure on the feed side and the vacuum pressure at the permeate chamber. For mass transfer of a single gas, the resistance caused by molecular - molecular collision within the pores is neglected. The gas will permeate through the membrane only if there is a total pressure drop across the pores. Table 1 shows the mass transfer mechanisms based on the Kn values in porous membranes.

Table 1
Mass transfer mechanism in membrane pore

Total pressure difference	Kn<0.01	0.01<Kn<1	Kn>1
$\Delta P \neq 0$	Poiseuille flow	Poiseuille flow-Knudsen diffusion transition mechanism	Knudsen diffusion

As Kn calculated from Eq. (1) is in the range of 0.11- 0.55 for water vapour ($0.2 \leq d \leq 1.0$ μm [16], $l \approx 0.11$ μm at 60 °C [17]), the dominating mass transfer mechanism within the pores is Poiseuille flow-Knudsen diffusion transition mechanism [4, 17]. Therefore, the mass transfer ($N_{K\text{-}P}$) across the membrane in VMD can be expressed as [4]:

$$N_{K-P} = N_K + N_P \tag{2}$$

where N_P and N_K represent the contribution of Poiseuille flow and Knudsen diffusion to mass transfer, respectively.

$$N_{K-P} = \left(\frac{8}{3} \frac{r\varepsilon}{b\tau} \sqrt{\frac{1}{2\pi RMT}} + \frac{r\varepsilon^2}{b\tau} \frac{1}{8\eta} \frac{P_m}{RT} \right) \Delta P \tag{3}$$

where R is the universal gas constant, T is the mean temperature in the pore, M is the molecular mass, r is the radius of the pore, η is the viscosity of the gas transferred across the membrane pores, b is the thickness of the membrane ($b = r_i \ln(r_o / r_i)$) for hollow fibre membrane), r_i and r_o are the inner and outer radii of the hollow fibre, ε is the porosity of the membrane, τ is the tortuosity factor of the pores, $P_m = (P_{vapour} + P_{vacuum})/2$ is the mean pressure in the pores and $\Delta P = P_{vapour} - P_{vacuum}$ is the pressure difference between the feed and permeate interfaces. If we define:

$$a_0 = \frac{r\varepsilon}{b\tau}, \text{ and } b_0 = \frac{r\varepsilon^2}{b\tau} \tag{4}$$

which depend on the characteristics of the membrane, then,

$$N_{K-P} = \left(\frac{8}{3} a_0 \sqrt{\frac{1}{2\pi RMT}} + b_0 \frac{1}{8\eta} \frac{P_m}{RT} \right) \Delta P \tag{5}$$

From Eq. (5), it can be found that if a_0 and b_0 are available, the mass transfer in VMD can be calculated. Theoretically, a_0 and b_0 can be measured by the gas permeation as presented by Lei [4], in which the pressure difference (ΔP) is set as constant and the flux varies with the mean pressure in the pores (P_m). Therefore, Eq. (5) can be expressed as:

$$N_{K-P} = A_0 + B_0 P_m \tag{6}$$

where $A_0 = \frac{8}{3} a_0 \sqrt{\frac{1}{2\pi RMT}} \Delta P$, and $B_0 = b_0 \frac{1}{8\eta RT} \Delta P$. If N_{K-P} is plotted against P_m, A_0 and B_0 are respectively the intercept and the slope of the straight line, from which a_0 and b_0 can be calculated by cancelling specific experimental conditions. From Eq. (5), only two parameters a_0 and b_0, instead of four parameters: the porosity ε, tortuosity τ, pore size r and the thickness b of the membrane, are required for calculating the flux for VMD.

2.2 Heat transfer

For hollow fibre VMD modelling, the heat balance of the feed stream from the bulk to the boundary layer can be expressed as:

$$Q_{f,transfer} = \alpha_f (T_f - T_1) W dx = N_{K-P} H_{latent} W dx + \frac{\lambda}{b} (T_1 - T_2) W dx \tag{7}$$

where $Q_{f,transfer}$ is the absolute overall heat transfer, $W = 2\pi r_i$ is the inner circumference of the hollow fibre, H_{latent} is the latent heat of the permeate, α_f is the convective heat transfer coefficient, λ is the thermal conductivity of the hollow fibre, and T_1 and T_2 are the interface temperature of the hollow fibre membrane on feed and permeate sides. Thermal conductivity can be calculated by Eq. (8) [4, 6, 18-20] :

$$\lambda = \varepsilon \lambda_{vapour} + (1 - \varepsilon) \lambda_{solid} \tag{8}$$

where λ_{vapour} and λ_{solid} are the thermal conductivities of the vapour in the pores and the membrane material, respectively. In VMD, because both the absolute pressure and thermal conductivity of the vapour are very low (λ_{vapour} = 0.016 $Wm^{-1}K^{-1}$ [21, 22] at atmospheric pressure), the λ_{vapour} compared to λ_{solid} (~0.16 $Wm^{-1}K^{-1}$) in this study is negligible. Therefore, the thermal conductivity of the hollow fibre is about 0.024 $Wm^{-1}K^{-1}$ (the porosity of the hollow fibre membrane used was 85%) which is half of membrane thermal conductivity under atmospheric pressure. In a DCMD study [12, 13, 18], the sensible heat loss was about 30% of the overall energy loss from the feed stream, when a flat sheet membrane with a thermal conduction coefficient (λ/b) of 900 $Wm^{-2}K^{-1}$ was used. The thermal conduction coefficient of the hollow fibre membrane (b = 280 μm) used in this study was about 86 Wm^{-}

$^{2}K^{-1}$, one tenth that of the flat sheet membrane. Therefore, the sensible heat loss was estimated to be less than 3% of that for VMD (the shell side is also under vacuum rather than liquid in DCMD). Therefore, the sensible heat loss can in generally be neglected in the VMD heat balance calculation [4, 23, 24].

The convective heat transfer coefficient can be calculated from [25]:

$$\alpha_f = \frac{Nu\lambda_w}{d_i} \tag{9}$$

where Nu is Nusselt number, d_i is the inner diameter of the hollow fibre and λ_w is the thermal conductivity of the water.

Since in this study the ratio of the membrane length to membrane inner diameter is 312.5, greater than 100, for the fully developed laminar flow in this study (Reynolds number in range of 600 to 3800), a constant Nusselt number of 4.364 was used based on Shah and London's finding [26].

Since the driving force of VMD is the pressure difference between the saturated vapour pressure at temperature of T_1 and the vacuum pressure on the shell side. If the vacuum pressure is given, the temperature polarisation of the feed will affect the mass transfer driving force, which can be assessed by:

$$TPC = \frac{T_1 - T_2}{T_f - T_p} \tag{10}$$

Here, TPC is the coefficient of temperature polarisation on the feed side. T_2 can be considered approximately equal to T_p in VMD due to the low absolute pressure and very fast vapour velocity (about 69 m/s based on 40% packing density module and absolute pressure 2 kPa), and can be estimated by the Antoine equation [3, 4, 27, 28] based on the experimental findings.

2.3 Procedures for solving modelling equations. The modelling program was developed using Visual Basic based on the mass and energy balances. The flow chart is shown in Figure2.

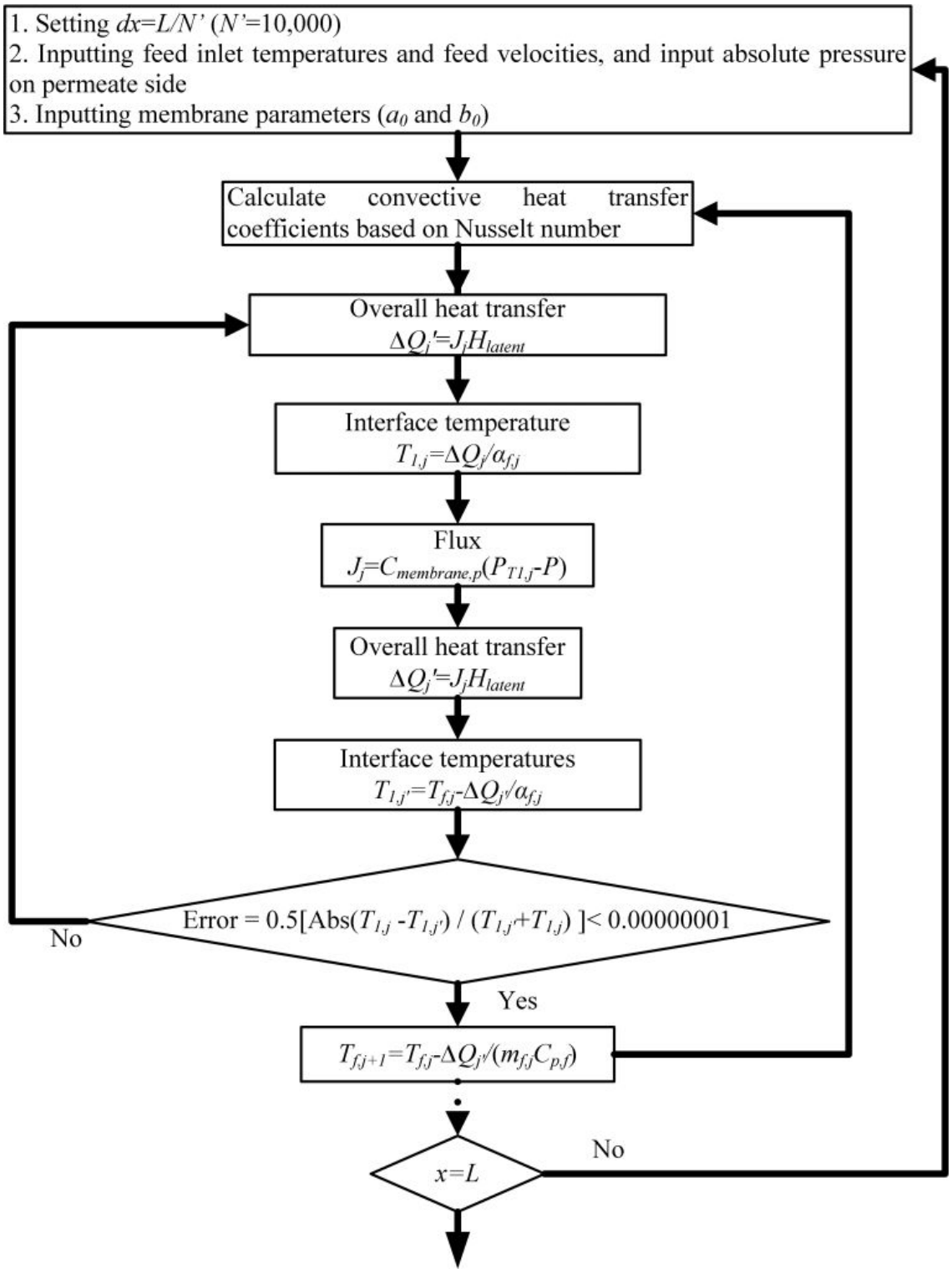

Figure 2 VMD modelling program flow chart

3. Experimental

3.1 Gas permeation

The setup for gas permeation test is shown in Figure 3 in which a dead end hollow fibre module and nitrogen were employed. The test gas inlet gauge pressure varied in the range of 5 - 70 kPa. The transmembrane pressure difference between the gas feed inlet and gas permeate outlet of the hollow fibre module was set at 2.00 ± 0.01 kPa to reduce compressibility of the membrane and the flux - length dependency. A digital manometer (645, TPI) was used for feed inlet pressure measurement and for monitoring the pressure difference between the feed and permeate streams. The gas flowrate was measured by timing a soap bubble passing through a soap flow meter (100 mL). Two pieces of hollow fibre samples (Sample 1 and sample 2) were randomly selected for testing. The membrane sample was sealed in a 6 mm rigid nylon tube using epoxy resin, with one open end connected to the gas supply and the other end closed. For each fibre sample, gas permeation of 3 or 4 lengths were measured by preparing test fibre samples of varying length.

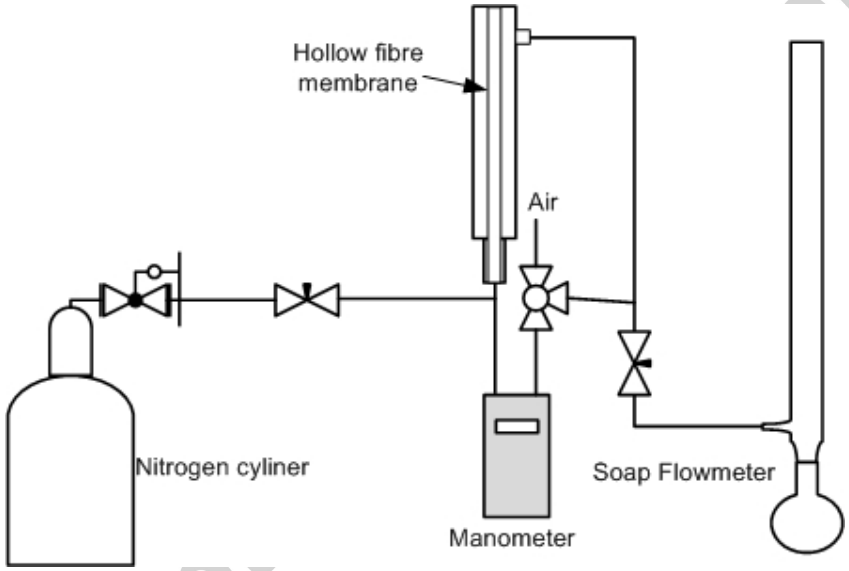

Figure 3 Gas permeation setup

3.2 VMD testing

3.2.1 Membrane modules

Three membrane modules with different packing densities were assembled as listed in Table 2. The hollow fibre membranes were encased in a 25 mm diameter polyethylene pipe, 25 cm in length and sealed in end caps made from tee fittings. The effective length of the hollow fibre membrane used was the same as the polyethylene pipe. The inner and outer diameters of the hollow fibre membrane were 0.8 and 1.6 mm respectively. The LEP of the hollow fibre measured with the method from [18] was 185±10 kPa.

Table 2
Specification of the fabricated modules

Packing density (%)	32	40	48

Fibre pieces	63	80	97

3.2.2 Conditions employed for verifications

Figure 4 shows a schematic diagram of the experimental setup. The feed stream was circulated by a pump and heated to the set temperature by a heater before entering the lumen side of the hollow fibre. The shell side of the module was subjected to negtive pressure by a vacuum pump, and the feed flowed through the lumen side of the membrane. Three thermometers were used to monitor the temperatures of feed inlet, feed outlet and module shell (permeate side). Two manometers were used to detect the pressure on the shell side of the module and pressure in the buffer tank, and the pressure in the shell was controlled by the control valve connected directly to the buffer tank. The flowrate of the feed stream was recorded by a flowmeter and was controlled by a flow control valve. The water vapour was condensed in a heat exchanger using 3.6ºC chilled water. The condensate was pump out by a peristallic pump from the permeate tank. A buffer tank was used to control the vacuum pressure and retain condensate that overflowed from the permeate tank. Salt rejection was monitored batchwise by a conductivity meter, and was greater than 99% in all experiments.

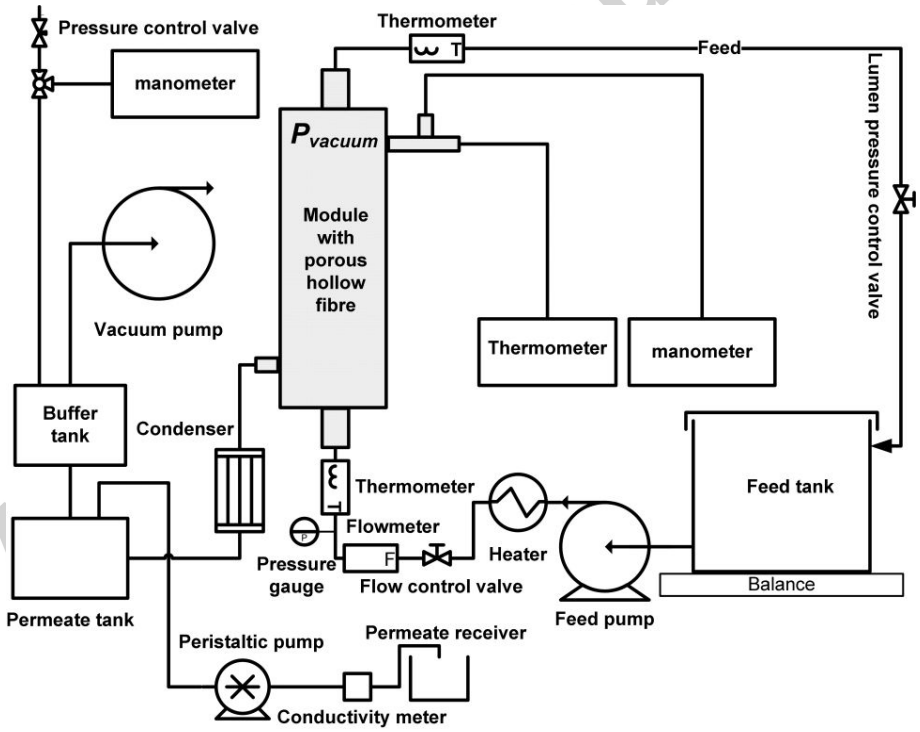

Figure 4 Schematic diagram of the experimeatal setup

Five or six different velocities (0.40 -2.56 m/s) and four different temperatures (40 - 70ºC) were tested for each module. The experimental data were collected at steady state (i.e. temperature varied within ±2ºC, velocity ±0.05 m/s, and absolute pressure ±1 kPa). The mean flux was calculated based on the weight loss of a covered feed tank over a duration of 1 - 2 h.

The flux in 10 - 20 min was also calculated and a variation of about ±5% around the mean flux was found.

4. Results and discussion

4.1 Gas permeation test

Figures 5-6 show the gas permeation and A_0 and B_0 values from membranes of different lengths. In Figure 6, both A_0 and B_0 showed membrane length dependency for the gas permeation test (A_0 increasing with length and B_0 decreasing with length). However, as described in Eqs. 5 and 6, A_0 and B_0 should be independent of membrane length. The observed dependency is due to the linear fitting of the gas permeation against pressure difference between the gas inlet and outlet. However, the inlet pressure difference is actually greater than the average pressure drop driving the gas through the membrane, because of the pressure distribution between the inlet and the dead end of hollow fibre. That is, the pressure drop along the lumen of the fibre leads to a change in pressure drop across the fibre as the shell side pressure is constant while the lumen side pressure varies with position along the fibre as has been inducted for liquid systems. Therefore, as the membrane becomes shorter, the average driving pressure approaches the gas inlet pressure. This phenomenon can also be found in Fig. 5, for tested lengths of Sample-1 and Sample-2 (except for Sample-2, 177 mm) where the shorter hollow fibre lengths showed higher gas permeation than that of the longer fibres due to a greater average driving pressure along the membrane. However, it also can be found from this figure that the rate of permeation increase reduced as the membranes became shorter.

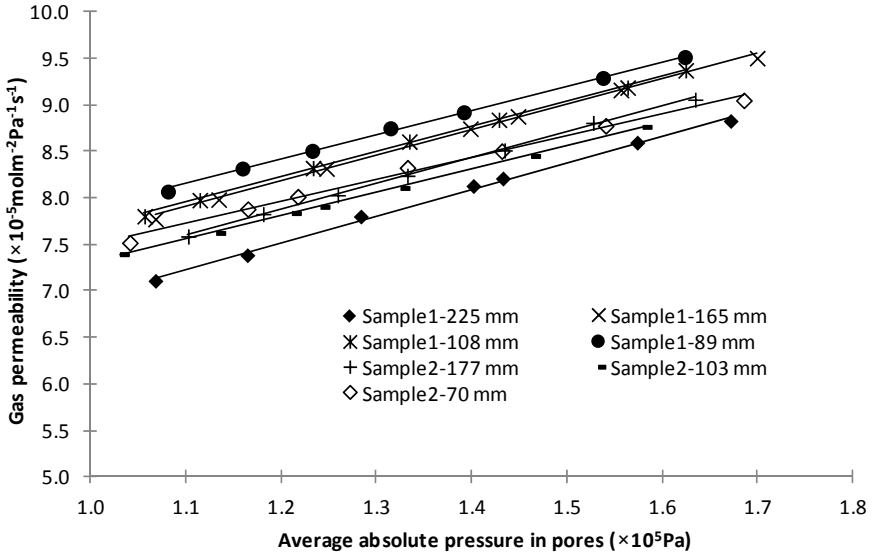

Figure 5 Gas permeation for hollow fibre

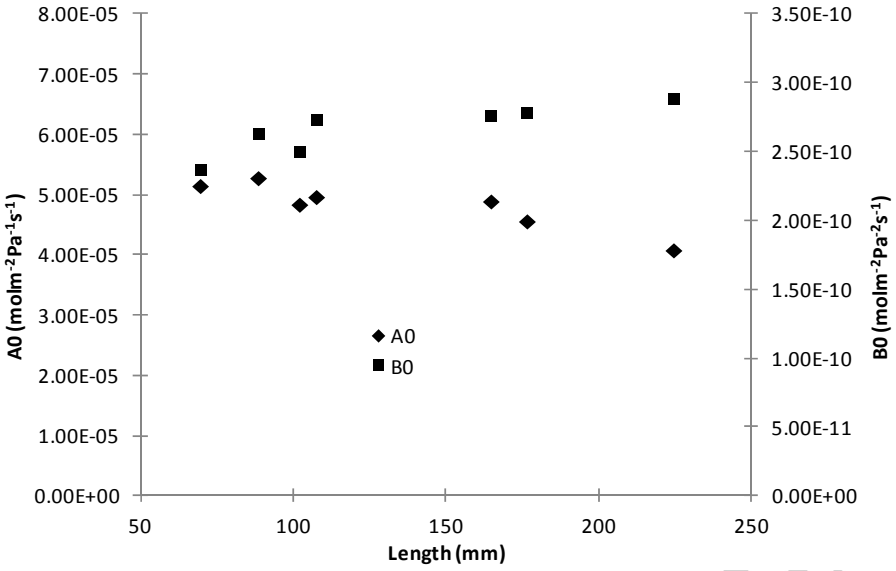

Figure 6 A_0 and B_0 varied with membrane lengths

To eliminate the length dependency, mathematical equations fitting the experimental data were determined with different fitting methods, in which the length was set as the independent variable and the measured A_0 and B_0 values were set as dependent variables. The theoretical values of A_0 and B_0 were calculated by extrapolating the membrane length (variable) to 0, as this represents the material property devoid of length effects. For the obtained data, fitting methods with correlation coefficient greater than 0.9 (Reciprocal Quadratic, Linear Fit, Quadratic Fit, Gaussian Model, and Reciprocal Model) were employed in the calculation of A_0 and B_0.

Table 3
Range of A_0 and B_0 at zero length calculated from the different fitting methods

A_0 ($\times 10^{-5}$ mol m^{-2} Pa^{-1}s^{-1})	B_0 ($\times 10^{-10}$ mol m^{-2} Pa^{-2}s^{-1})
5.0 - 5.7	2.24 - 2.29

4.2 Dependency of modelling on the variations of A_0 and B_0

As shown in Table 3, the A_0 and B_0 values at zero length extrapolated from different fitting equations were different. Therefore, it was necessary to assess the sensitivity of the modelling results from the variations of A_0 and B_0. In Table 4, the modelling results listed are based on the listed experimental conditions and the minimum and maximum values of the A_0 and B_0 selected from the calculated results of these fitting methods.

Table 4
Comparison of modelling results using different A_0 and B_0 (Permeate absolute pressure = 3 kPa)

Coefficients	Flux ($L\ m^{-2}h^{-1}$)			
	T_{fi} = 40 °C V = 0.92 m/s	T_{fi} = 70 °C V = 0.92 m/s	T_{fi} = 60 °C V = 0.4 m/s	T_{fi} = 60 °C V = 2.1 m/s
$A_0 = 5.0\times10^{-5}$ $B_0 = 2.29\times10^{-10}$	7.75	40.85	22.63	33.31
$A_0 = 5.0\times10^{-5}$ $B_0 = 2.24\times10^{-10}$	7.75	40.83	22.62	33.29
$A_0 = 5.7\times10^{-5}$ $B_0 = 2.24\times10^{-10}$	8.29	42.82	23.63	35.40
$A_0 = 5.7\times10^{-5}$ $B_0 = 2.29\times10^{-10}$	8.29	42.84	23.63	35.42
Average	8.02	41.84	23.13	34.36

It can be seen from Table 4 that the predicted flux only varied by ±2 - 3% around the average value under different conditions as A_0 and B_0 changed from the minimum to the maximum values determined from different curve fitting methods. This is less than the experimental variation, estimated as ±5%.

4.3 Experimental assessment of the modelling

Since the influence of the A_0 and B_0 values from the different fitting equations on the predicted results was less than the experimental variation, it was not possible to identify which fitting curves in the estimation of A_o and B_o were the most appropriate. Therefore, results from the linear fitting of the data in Figure 6, $A_0 = 5.7\times10^{-5}$ ($a_0 = 4.4\times10^{-4}$) and $B_0 = 2.26\times10^{-10}$ ($b_0 = 7.7\times10^{-11}$) were selected for subsequent assessment, as this represents the simplest extrapolation approach.

4.3.1 Assessment of modelling with varied feed velocities

Figure 7 presents both experimental and predicted results of flux varying with velocity. Although the three modules have different packing densities, the flux (both modelling and experimental results) was very similar under the same conditions, which was different from DCMD [29]. The lack of flux dependency on module packing density was due to the negligible temperature polarisation on the shell side of the module. The hollow fibre bundle has very low mixing resistance to the vapour compared to liquid, and therefore water vapour will be drawn away quickly from the membrane surface under low pressure (1- 3 kPa) to provide a uniform temperature distribution in the module. However, on the shell side of the DCMD (outside of the hollow fibre), the mixing resistance of the hollow fibre bundle to the liquid is much higher than to that of the vapour, and this resistance is due to the geometric structure (packing density) [26, 30]. Therefore, the variation of the packing density will alter

the driving force (temperature difference) for mass transfer in DCMD and hence change the flux.

The flux of VMD shows an asymptotic trend similar to DCMD [18], which increased quickly at low velocity and plateaued at high velocity. This trend is caused by both the reduced temperature polarisation of the feed stream with increasing velocity and increased average temperature of the feed stream [18].

In comparison with the 5% experimental variation around the mean value, the error between the predicted and the experimental results were similar and fell in the range of 0 - 5%. Therefore, the modelling results aligned with the experimental results quite well under experimental conditions with varying feed velocity.

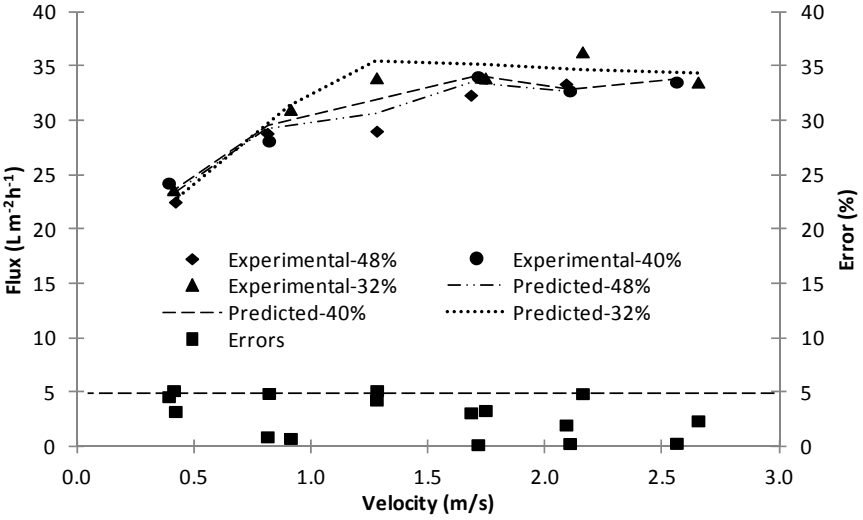

Figure 7 Comparison of predicted flux with initial experimental flux at different feed velocities and different packing densities
(Feed inlet temperature = 60 ± 2 ˚C, permeate absolute pressure = 2 ± 1 kPa)

The influence of feed velocity on temperature polarisation (Eq. (10)) and heat transfer coefficient (calculated based on Eq. (7)) on the feed side are shown in Figure 8. As the feed velocity increased from 0.4 to 2.1 m/s, the heat transfer coefficient only increased by 1.1% (from 3566 to 3604 W/m^2) due to the constant Nusselt number (Eq. (9)), and *TPC* decreased by 4.06% (from 0.0.841 to 0.807). The slight increase of the heat transfer coefficient was due to the increased heat conductivity of water at higher temperature [31]. Therefore, the observed flux increase in Figure 7 was largely due to the greater average feed temperature at higher velocity (higher feed outlet temperature) due to lower residency time of feed in the module. The slightly deceased *TPC* was due to increased flux based on Eq. (7).

Furthermore, since the hydrodynamic conditions do not have such a large effect on flux for VMD as they do for DCMD [18, 32], the factors dominating mass transfer will be the resistance to vaporisation (membrane permeability) and the vacuum pressure on the shell side at a given feed inlet temperature.

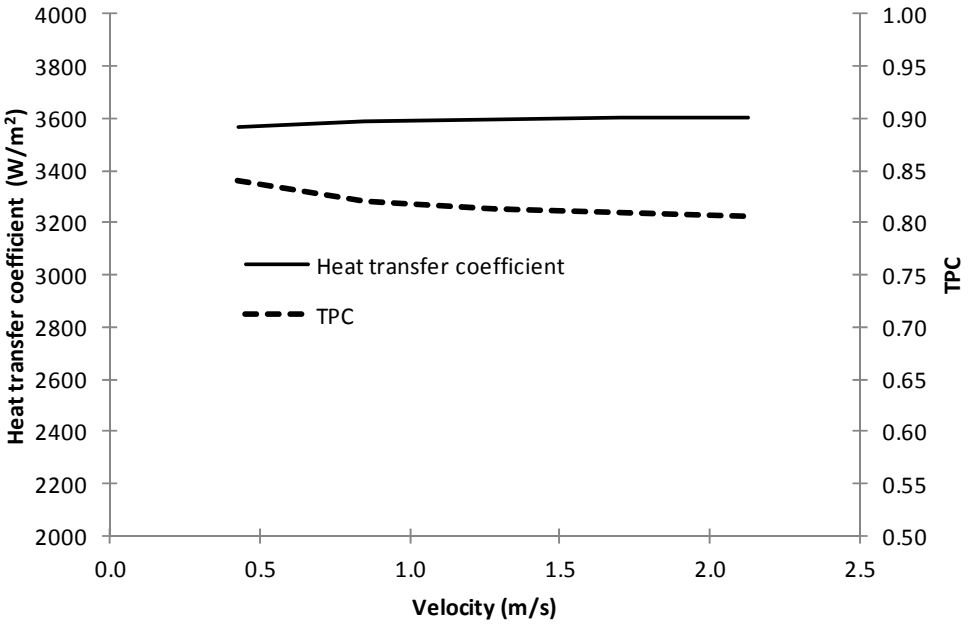

Figure 8 Predicted mean TPC and heat transfer coefficient at different feed velocities (Feed inlet temperature = 60 ˚C, permeate absolute pressure = 2 kPa, Packing density = 40%)

4.3.2 Assessment of modelling with varied feed temperatures

In Figure 9, the model predictions were assessed at different temperatures by comparing with the experimental results. Theoretically, there should be an exponential relationship between the flux and the temperature in VMD which is similar to that of DCMD [19, 33], due to the relationship between vapour pressure and temperature. However, the curves in Figure 9 show a more linear (R^2 ~ 0.99) than exponential (R^2 ~ 0.97) relationship between the flux and temperature. This was caused by an increased absolute pressure on the shell side at higher temperature (increased from 2.1 to 5.7, 2.1 to 4.8, and 1.3 to 3.1 kPa respectively for modules with packing densities of 48%, 40% and 32% as temperature increased from 40 to 70 ˚C), due to the capacity of the vacuum pump and the chiller. Therefore, the experimental pressure on the permeate side was not constant between experiments and this effected the resultant driving force across the membrane as well as the temperature. Again, the flux was independent of the module packing density, although the flux of the module with 32% packing density was higher than others due to the lower pressure (1.3 kPa) on the shell side at 40 °C.

The errors between the experimental and predicted results were around 5% for most of the results, while the errors for the two experiments at 70 °C were greater than 5% but less than 10%. This phenomenon may be due to that fact that more water was evaporated from the feed tank (not completely sealed) at the higher temperature (vapour pressure of 70 °C is 1.7 times of that of 60 °C). The error of the predicted results for higher packing density module is

smaller compared to that of the lower packing density module at high temperature, perhaps because the influence of evaporation (which can be considered constant) became less when using a higher packing density module due to the reduced ratio of evaporation rate to produced permeate (kg/h).

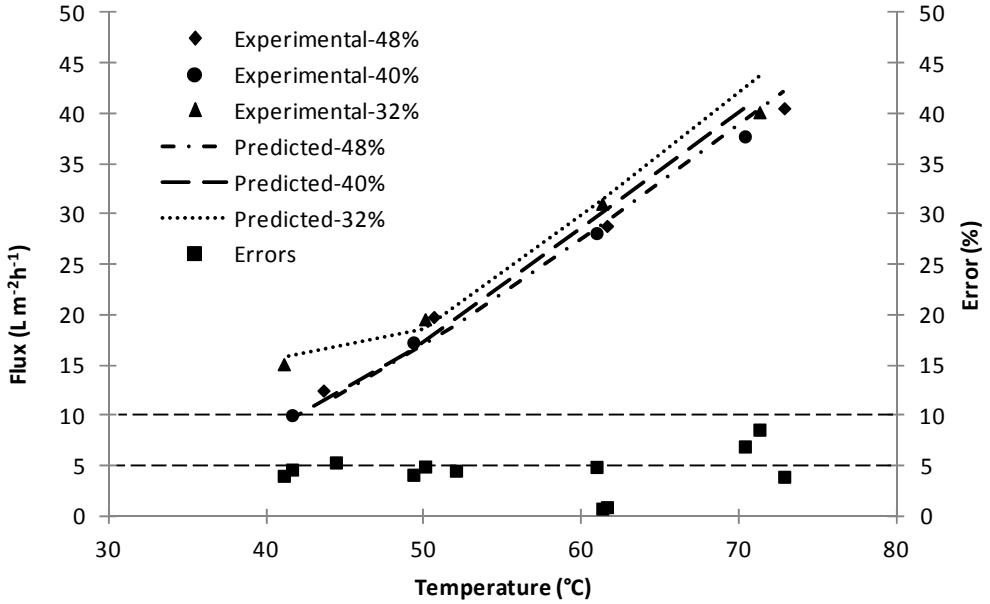

Figure 9 Comparison of predicted flux with initial experimental flux at different temperatures (velocity = 0.8 m/s, permeate absolute pressure = 2 – 5 ± 1 kPa)

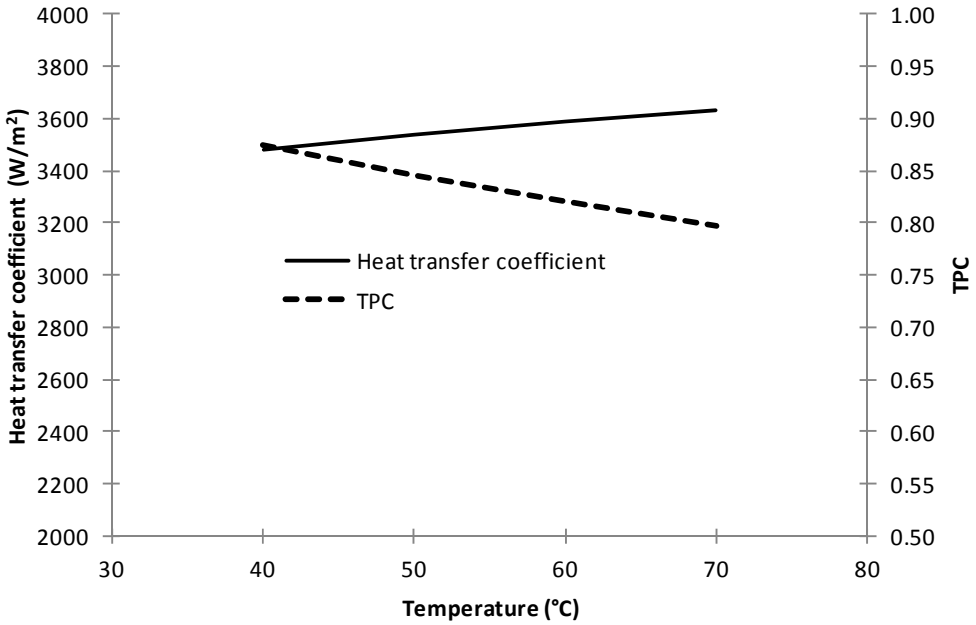

Figure 10 Predicted *TPC* and heat transfer coefficient at different feed inlet temperature (Feed velocity = 0.8 m/s, permeate absolute pressure = 2 kPa, Packing density = 40%)

In Figure 10, as the temperature increases from 40 to 70 °C, *TPC* declines by ~8.7% (from 0.87 to 0.95) and heat transfer coefficient increases by ~4.3% (3480 to 3630 W/m^2). The increased heat transfer coefficient arises from increased thermal conductivity at higher average temperature [31]. Based on Eqs. (7) and (10), it can be found that the reduced *TPC* is also mainly because of the increased thermal energy demand when the flux becomes greater at higher temperature.

5. Conclusion

A new method of measuring the properties of hollow fibre membranes for VMD modelling was developed. Measuring the gas permeability as a function of membrane length and extrapolating to zero length allowed A_0 and B_0 for the membrane material to be determined. These values resulted in predicted VMD flux within the experimental error for different velocities. For various temperatures considered, the predicted results at different temperatures were mostly in the experimental variation range. However, the error was greater at 70˚C, perhaps due to water evaporation in the feed tank (the flux was calculated based on weight loss of feed tank). Additionally from both the modelling and experimental results, the flux in VMD was independent of the module packing density under the current experimental conditions. The assessment shows that the mathematical models predictions agree well with the experimental results of short experimental duration (1 - 2 h). Longer term experiments may be needed for further assessment.

Acknowledgements

The authors acknowledge the financial support of the National Centre of Excellence for Desalination Australia which is funded by the Australian Government through the Water for the Future initiative.

6. Nomenclature

A	Membrane area (m^2)
A_0, B_0	Membrane mass transfer coefficients (mol m^{-2} Pa^{-1}s^{-1}, mol m^{-2} Pa^{-2}s^{-1})
C_p	Heat capacity (J/mol.K)
D_H	Hydraulic diameter of tubing/membrane (m)
Kn	Knudsen number
l	Molecular path (μm)
L	Hollow fibre length (m)
d	Pore diameter (μm)
λ	Thermal conductivity (W/m)
M	Molecular weight (g/mol)
Nu	Nusselt number
N_P, N_K	Poiseuille flow and Knudsen diffusion (mol/s)

P	Pressure (Pa)
Pr	Prandtl number
R	Gas constant (J/mol.K)
Re	Reynolds number
T	Temperature (K)
TPC	Coefficient of polarisation on feed side
v	Linear velocity (m/s)
$Q_{f,transfer}$	absolute overall heat transfer (W)
r	Pore radius (μm)
W	Circumference of the hollow fibre (m)
μ	Liquid dynamic viscosity (Pa.s)
ε	Porosity
Subscript	
c	Cold side
$1,2$	Feed and permeate interfaces
f	Feed
h	Hot side
fi	Feed inlet
fo	Feed outlet
in	Inlet
out	Outlet
p	Permeate

References

[1] F. Banat, R. Jumah, M. Garaibeh, Exploitation of solar energy collected by solar stills for desalination by membrane distillation, Renewable Energy. 25 (2002) 293-305.
[2] P. K. Weyl, Recovery of demineralized water from saline waters, U. S. A, (1967).
[3] K. W. Lawson, D. R. Lloyd, Membrane distillation, Journal of Membrane Science. 124 (1997) 1-25.
[4] Z. Lei, B. Chen, Z. Ding, Membrane distillation, in: Z. Lei, B. Chen, Z. Ding (Z. Lei, B. Chen, Z. Dings), Special Distillation Processes, Elsevier Science, Amsterdam, 2005, pp. 241-319.
[5] K. Schneider, T. J. van Gassel, Membrandestillation, Chemie Ingenieur Technik. 56 (1984) 514-521.
[6] E. Curcio, E. Drioli, Membrane Distillation and Related Operations: A Review, Separation and Purification Reviews. 34 (2005) 35 - 86.
[7] M. Gryta, Fouling in direct contact membrane distillation process, Journal of Membrane Science. 325 (2008) 383-394.
[8] A. Hanafi, Desalination using renewable energy sources, Desalination. 97 (1994) 339-352.
[9] J. Tonner, Barriers to Thermal Desalination in the United States, Desalination and Water Purification Research and Development Program Report No. 144, (2008).
[10] A. O. Imdakm, M. Khayet, T. Matsuura, A Monte Carlo simulation model for vacuum membrane distillation process, Journal of Membrane Science. 306 (2007) 341-348.
[11] J. Woods, J. Pellegrino, J. Burch, Generalized guidance for considering pore-size distribution in membrane distillation, Journal of Membrane Science. 368 (2011) 124-133.
[12] J. Zhang, S. Gray, J.-D. Li, Modelling heat and mass transfers in DCMD using compressible membranes, Journal of Membrane Science. 387–388 (2012) 7-16.
[13] J. Zhang, J.-D. Li, S. Gray, Effect of applied pressure on performance of PTFE membrane in DCMD, Journal of Membrane Science. 369 (2011) 514-525.
[14] A. O. Imdakm, T. Matsuura, A Monte Carlo simulation model for membrane distillation processes: direct contact (MD), Journal of Membrane Science. 237 (2004) 51-59.

[15] J. Zhang, J.-D. Li, M. Duke, Z. Xie, S. Gray, Performance of asymmetric hollow fibre membranes in membrane distillation under various configurations and vacuum enhancement, Journal of Membrane Science. 362 (2010) 517-528.
[16] A. M. Alklaibi, N. Lior, Membrane-distillation desalination: Status and potential, Desalination. 171 (2005) 111-131.
[17] J. Phattaranawik, R. Jiraratananon, A. G. Fane, Effect of pore size distribution and air flux on mass transport in direct contact membrane distillation, Journal of Membrane Science. 215 (2003) 75-85.
[18] J. Zhang, N. Dow, M. Duke, E. Ostarcevic, J.-D. Li, S. Gray, Identification of material and physical features of membrane distillation membranes for high performance desalination, Journal of Membrane Science. 349 (2010) 295-303.
[19] M. Qtaishat, T. Matsuura, B. Kruczek, M. Khayet, Heat and mass transfer analysis in direct contact membrane distillation, Desalination. 219 (2008) 272-292.
[20] P. Termpiyakul, R. Jiraratananon, S. Srisurichan, Heat and mass transfer characteristics of a direct contact membrane distillation process for desalination, Desalination. 177 (2005) 133-141.
[21] B. B. Spencer, H. Wang, K. K. Anderson, Thermal Conductivity of IONSIV® IE-911™ Crystalline Silicotitanate and Savannah River Waste Simulant Solutions, Oak Ridge Laboratory Oak (2000).
[22] J. V. Sengers, Representative Equations for the Thermal Conductivity of Water Substance, Journal of Physical Chemistry 13 (1984) 893-933.
[23] S. Bandini, G. C. Sarti, Concentration of must through vacuum membrane distillation, Desalination. 149 (2002) 253-259.
[24] S. Al-Asheh, F. Banat, M. Qtaishat, M. Al-Khateeb, Concentration of sucrose solutions via vacuum membrane distillation, Desalination. 195 (2006) 60-68.
[25] R. W. Serth, Process Heat Transfer: Principles and Applications, Elsevier Academic Press, 2007.
[26] J. P. Holman, Heat transfer, McGraw-Hill, 2002.
[27] M. Gryta, M. Tomaszewska, K. Karakulski, Wastewater treatment by membrane distillation, Desalination. 198 (2006) 67-73.
[28] K. W. Lawson, D. R. Lloyd, Membrane distillation. II. Direct contact MD, Journal of Membrane Science. 120 (1996) 123-133.
[29] M. Gryta, M. Tomaszewska, A. W. Morawski, A Capillary Module for Membrane Distillation Process, Chemical Papers. 54 (2000) 370-374
[30] A. F. Mills, Mass Transfer, Upper Saddle River, EUA : Prentice-Hall, 2001.
[31] M. L. V. Ramires, C. A. N. de Castro, Y. Nagasaka, A. Nagashima, M. J. Assael, W. A. Wakeham, Standard Reference Data for the Thermal Conductivity of Water, Journal of Physical and Chemical Reference Data. 24 (1995) 1377-1381.
[32] J. Zhang, M. Duke, E. Ostarcevic, N. Dow, S. Gray, J.-D. Li, Performance of New Generation Membrane Distillation Membranes, Water Science & Technology: Water Supply. 9 (2008) 501–508
[33] R. W. Schofield, A. G. Fane, C. J. D. Fell, Heat and mass transfer in membrane distillation, Journal of Membrane Science. 33 (1987) 299-313.

Highlights

- A mathematical model is developed for hollow fibre VMD using membrane permeability,
- Length dependency of the permeability of hollow fibre is minimised mathematically,
- Modelling results are assessed experimentally under various conditions, and
- Error analysis is conducted based on modelling and experimental conditions.